Cancer Cell, Volume *24*

Supplemental Information

A Core Human Primary Tumor Angiogenesis Signature Identifies the Endothelial Orphan Receptor ELTD1 as a Key Regulator of Angiogenesis

Massimo Masiero, Filipa Costa Simões, Hee Dong Han, Cameron Snell, Tessa Peterkin, Esther Bridges, Lingegowda S. Mangala, Sherry Yen-Yao Wu, Sunila Pradeep, Demin Li, Cheng Han, Heather Dalton, Gabriel Lopez-Berestein, Jurriaan B. Tuynman, Neil Mortensen, Ji-Liang Li, Roger Patient, Anil K. Sood, Alison H. Banham, Adrian L. Harris, and Francesca M. Buffa

Inventory of Supplemental Information

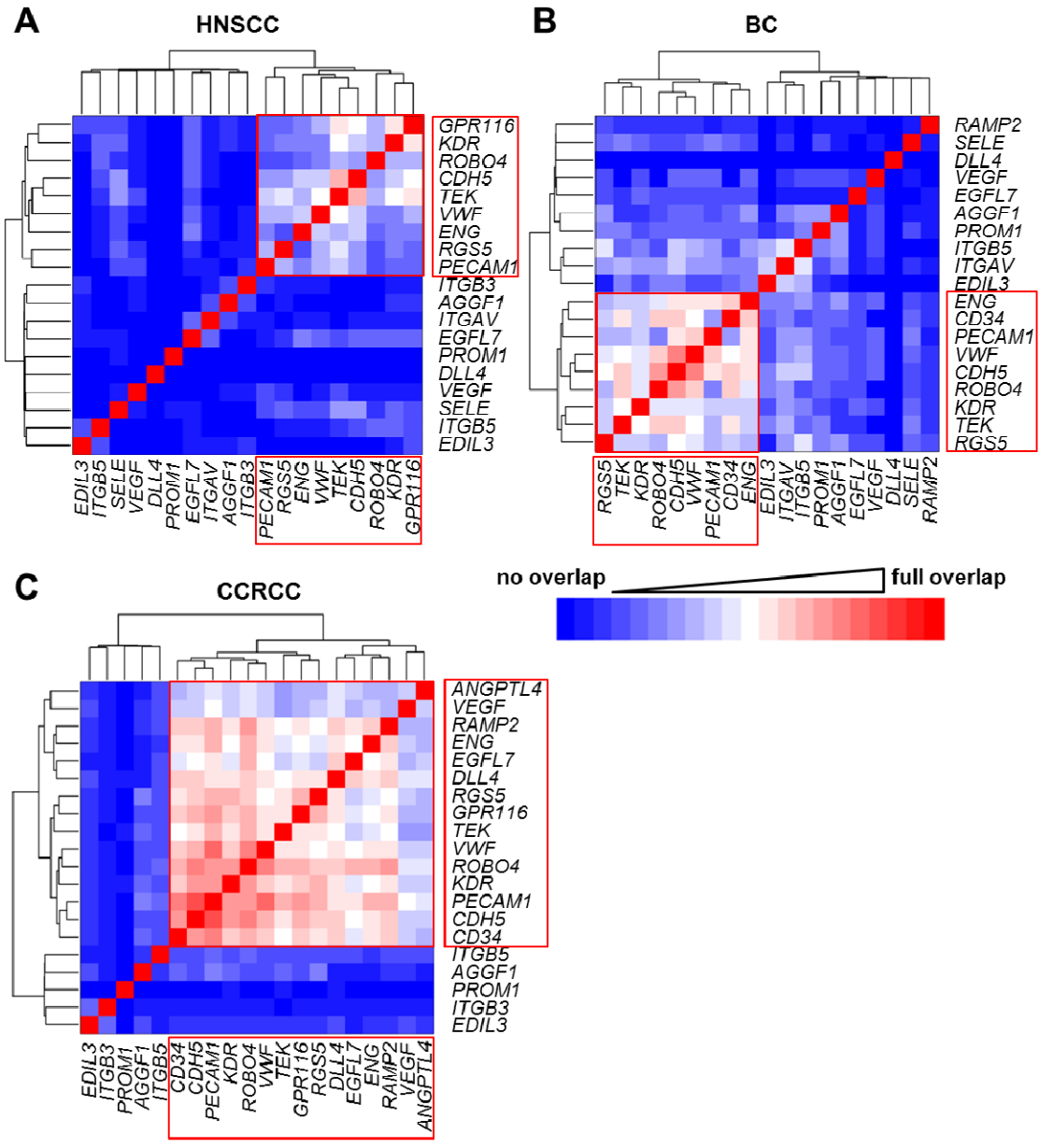

Figure S1, related to Figure1. Seed clustering to build an angiogenesis profile *in vivo* of genes regulated in primary tumors: overlap between seeds

Overlap amongst seed clusters that passed initial filtering in 121 head and neck squamous cell carcinomas (HNSCC) (A), 959 breast cancers (BC) (B) and 170 clear cell renal cell carcinomas (CCRCC) (C). Genes within red boxes are those with highly overlapping expression patterns that were then used to generate tumor type-specific angiogenesis meta-signatures. Datasets considered are shown in Table in Supplemental Experimental Procedures and details of initial filtering are provided in Material and Methods section. Color scale is shown on the right.

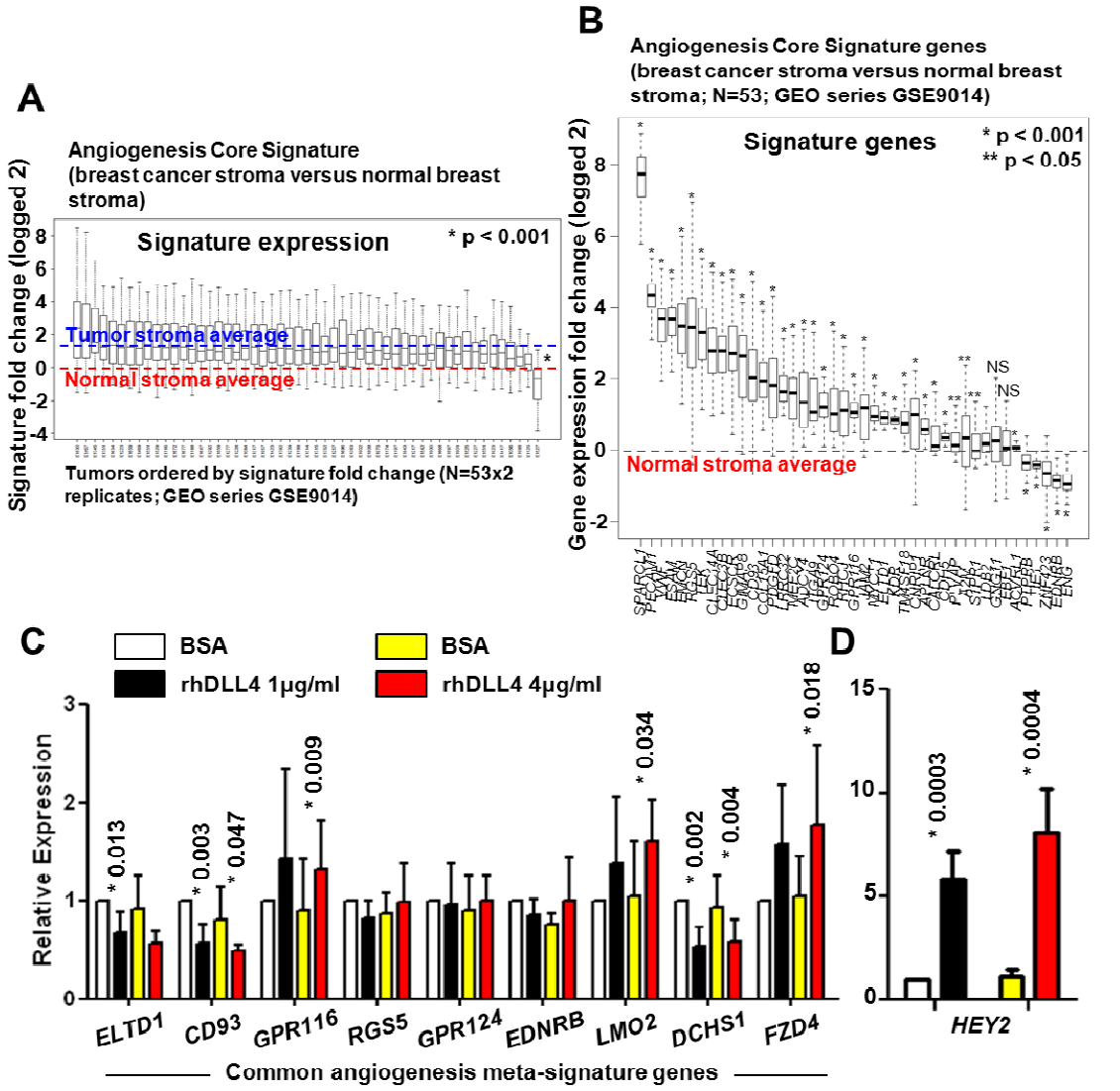

Figure S2, related to Figure 2. Upregulation of the common overexpressed core signature in human breast cancer stroma and regulation of selected genes by DLL4 in endothelial cells

(A) Expression analysis of the core signature showed significant upregulation in purified breast cancer stroma compared to normal (GSE9014; GEO database), average fold change between tumor stroma and normal tissue was 2.62 (linear scale, 1.39 when logged base2; t-test 2-sided). (B) Expression distribution in the 53 samples, boxplots are provided for each core signature gene in the same dataset used in (A) (relative to normal tissue level). The normalized and annotation datasets were downloaded from GEO, mean expression values were considered across replicate samples. Boxplots in (A) and (B) show the median value, and first and third quartiles. (C) Six genes from the core signature (*ELDT1, CD93, GPR116, RGS5, GPR124, EDNRB*) and 3 genes (*LMO2, DCHS1, FZD4*) from the extended common angiogenesis signature were selected and their expression analysed by qPCR in HUVEC stimulated for 16h with 2 different rhDLL4 concentrations. (D) qPCR analysis of a known NOTCH target gene. Bars represent means ±SD (n=6; paired t-test).

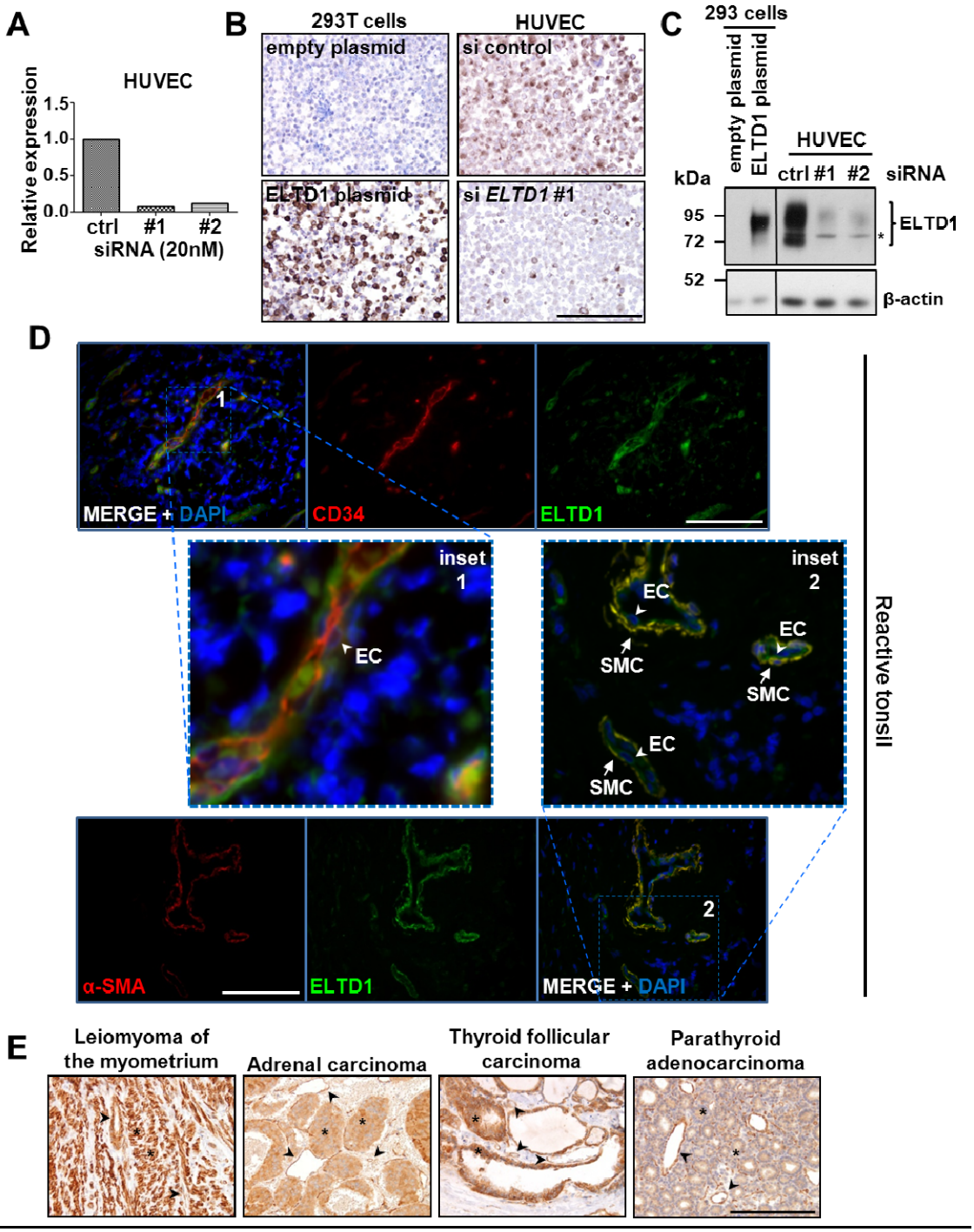

Figure S3, related to Figure 3. Gene knockdown, antibody validation and ELTD1 expression in human endothelial, smooth muscle and tumor cells

(A) qPCR analysis for ELTD1 performed on total RNA extracted from HUVEC 24h after transfection with 2 different *ELTD1* specific and 1 control (ctrl) siRNA. (B) IHC analysis of 293T cells transfected with control or ELTD1-coding plasmids and HUVEC transfected with control and *ELTD1* #1 siRNAs. 24h after transfection cell pellets were generated, paraffin-embedded and sectioned for IHC analysis. Scale bar: 200µm. (C) Western Blot analysis on similar transfectants as in (B). *Non-specific band appearing with long exposure. (D) Immunofluorescence analysis of reactive tonsil sections co-stained for ELTD1 in green and CD34 (EC marker) or

α-SMA (SMC marker) in red. Scale bars: 100µm. (E) Strong positivity by cancer cells was observed in some type of neoplasms (asterisks; positive vessels indicated by arrow heads). Scale bar: 200µm.

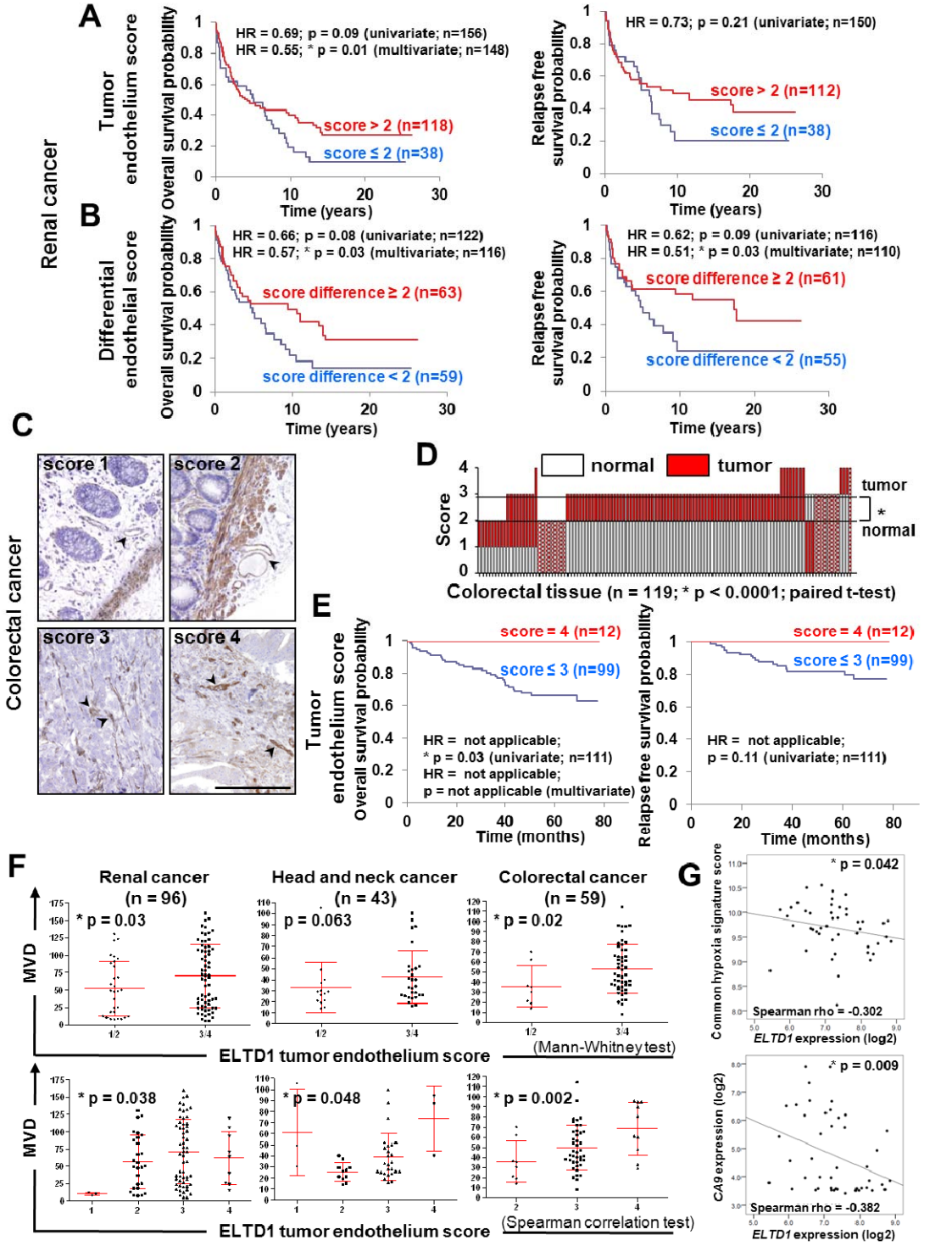

Figure S4, related to Figure 4. Endothelial ELTD1 expression and its clinico-pathological correlations

In renal cancer, EC ELTD1 score has borderline correlation with overall survival but no statistical relevance for relapse free survival (A) while the difference in score between tumor-associated and normal ECs shows

borderline statistical correlation with both overall and relapse free survival in renal cancer (B). (C) Representative IHC pictures of ELTD1 score categories (scores 1/2 are taken from normal colon while score 3/4 from colorectal cancer cases). Arrow heads indicate blood vessels. Scale bar: 20µm. (D) Summary of ELTD1 expression in 119 cases of colorectal cancer with normal matched colon. Each column represents a patient with red and white bars showing the score in tumor-associated and normal ECs respectively. (E) Higher tumor endothelial ELTD1 score shows significant correlation with better overall survival in univariate analysis (multivariate analysis not applicable). HR = Hazard Ratio. (F) Endothelial ELTD1 levels positively correlate with MVD in renal, head and neck and colorectal cancer (average MVD ±SD is highlighted). (G) *ELTD1* mRNA expression anti-correlates with a hypoxia gene signature and *CA9* levels in head and neck cancer.

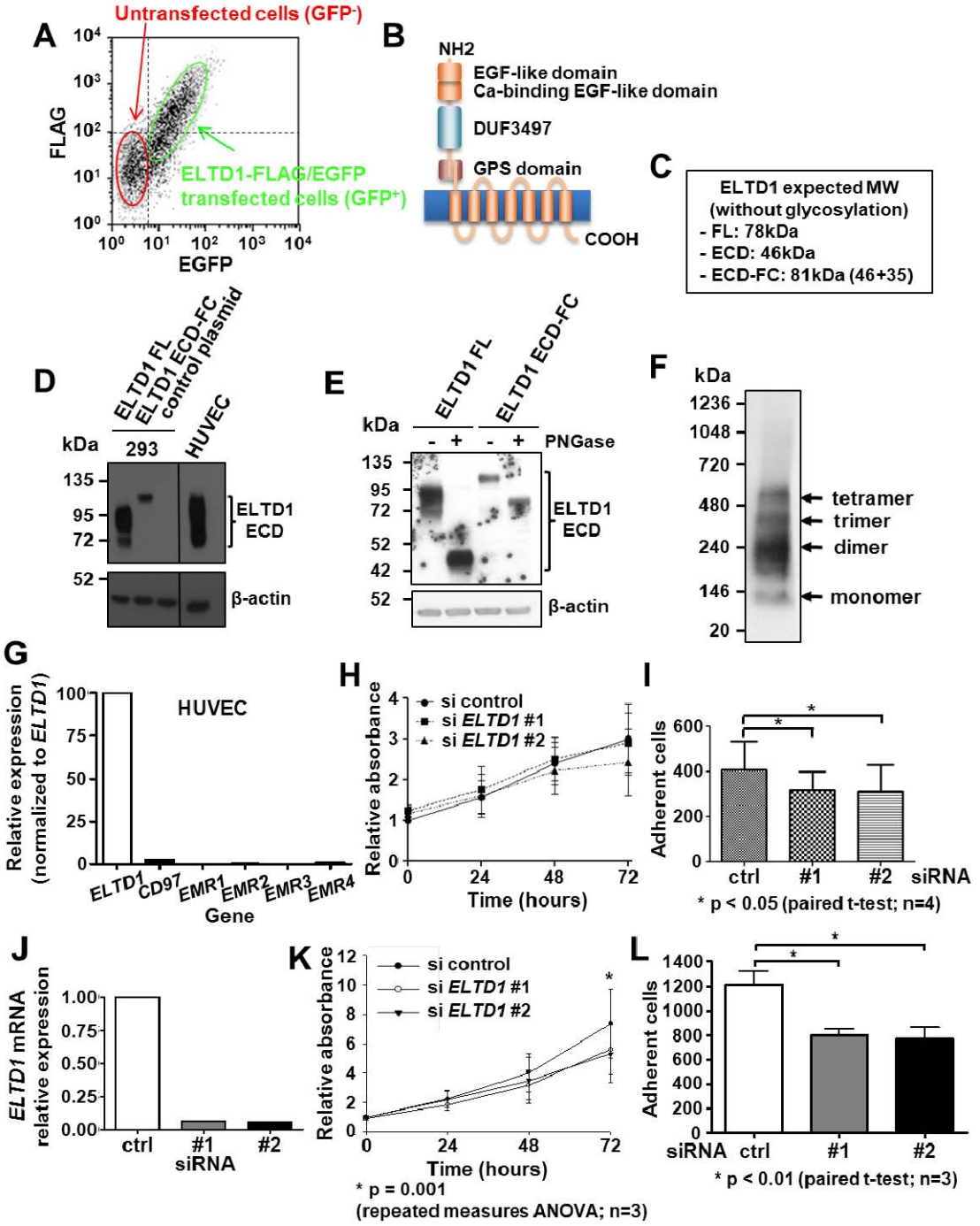

Figure S5, related to Figure 5. ELTD1 surface expression, Western blotting detection of ELTD1-ECD and functional consequences of ELTD1 silencing in HUVEC and HuVSMC *in vitro*.

(A) Flow cytometry analysis using anti-Flag antibodies to detect cell surface expression of ELTD1 in 293T cells transfected with a Flag-ELTD1/IRES/EGFP plasmid. Untransfected cells (GFP^-) in the same sample represent an internal negative control and do not express the Flag epitope on their surface. (B) Schematic structure of the ELTD1 protein. DUF3497, Domain of Unknown Function 3497; GPS, GPCR proteolisis site. (C) Expected MW for different ELTD1 proteins (without glycosylation). FL=Full length; ECD=Extracellular Domain. (D) Analysis of cell lysates from 293 transfected with plasmids coding ELTD1 FL, FC-coniugated ELTD1 ECD and control plasmid. HUVEC lysate was used as control. (E) PNGase treatment confirms that by WB we are detecting only the ELTD1 ECD since the MW observed after treatment for the ELTD1 FL (about 46kDa) matches the predicted size for the ECD and the MW observed for the ECD-FC (about 81kDa). (F) WB in non-denaturing conditions shows that HUVEC express 4 main bands compatible with the presence of ELTD1 monomers and multimers. (G) qPCR analysis of *ELTD1* family member expression levels in HUVEC. (H) Analysis of HUVEC viability after *ELTD1* silencing (graph represents the average ±SD; n=4). (I) Reduced HUVEC adhesion to matrigel was observed after *ELTD1* silencing (bars represent mean ±SD). (J) *ELTD1* silencing efficiency by qPCR in HuVSMC. (K) Analysis of *ELTD1* silenced HuVSMC viability shows a significant reduction 72h after transfection (graph represents average ±SD). (L) As for HUVEC, *ELTD1* silencing reduced HuVSMC adhesion to matrigel (bars represent average ±SD).

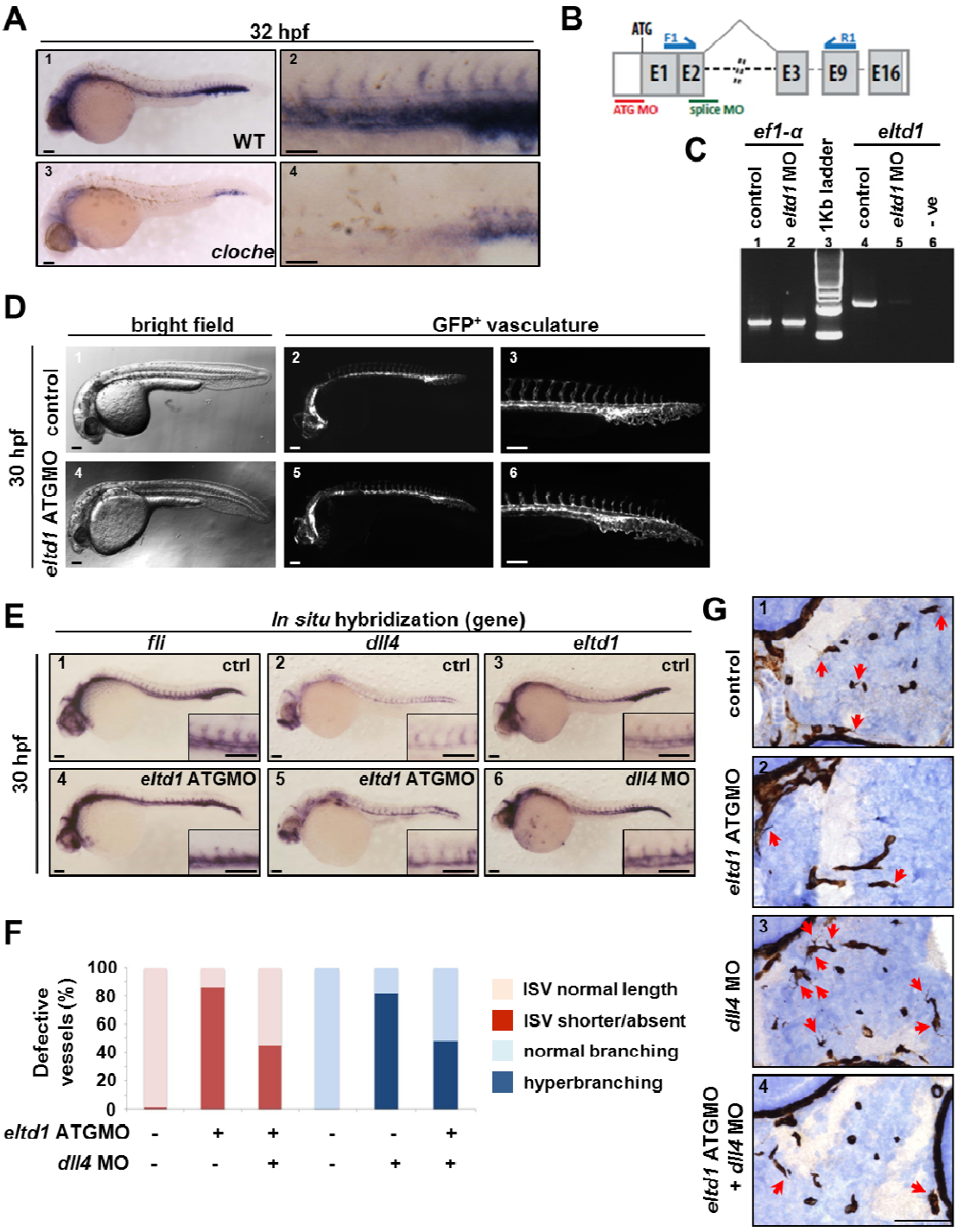

Figure S6, related to Figure 6. *Eltd1* in zebrafish: vascular expression pattern, morpholino design and silencing functional consequences

(A) *In situ* hybridization for the zebrafish *eltd1* homolog gene *zgc:63629* shows that, compared to WT embryos, *eltd1* expression is severely downregulated in a 32hpf *cloche* mutant, where blood and endothelial structures are compromised. Scale bars: 100 µm. (B) Genomic structure of zebrafish *eltd1* gene, with translated exons represented as grey boxes, untranslated sequences represented as white boxes and introns as dashed lines (exons 4 to 8 and 10 to 15 not represented due to space constraints). ATG and splice blocker MO binding sites are shown (red and green lines, respectively). *Eltd1* primers used in RT-PCR analysis (C) are shown (binding

sites represented as blue arrows). (C) RT-PCR analysis revealed a 1162bp *eltd1* product in 27hpf uninjected embryos (lane 4), while a severe downregulation of the product was detected in *eltd1* morphants (lane 5). Efficacy of cDNA synthesis was revealed by comparable *ef1-a* amplification in uninjected (lane 1) and morphant (lane 2) 27hpf embryo samples. Lane 3 shows 1Kb ladder and lane 6 the negative control. (D) Lateral views of Tg(kdrl:GFP) embryos at 30hpf. Endothelial cells sprouting from the DA to form the ISV is affected in *eltd1* morphants (D5, D6), when compared with uninjected controls (D2, D3). Scale bars: 100µm. (E) *In situ* hybridization showing *dll4* upregulation in 30hpf *eltd1* morphant embryos (E5) compared to uninjected control (ctrl; E2). Expression of *fli1* was not affected by *eltd1* gene silencing (E1 and E4). *Eltd1* expression is upregulated in 30hpf *dll4* morphants (E3 and E6). Scale bars: 100µm. (F) Quantification of the vascular defects in different morphants shows reciprocal phenotypic rescue between *eltd1* and *dll4* silencing. For each of the conditions tested, the percentage of embryos showing normal (normal length) or deficient (shorter/absent) ISV and normal (normal branching) or hyperbranching arteries (hyperbranching) is shown. Affected embryo percentages from one representative experiment are shown (N. of embryos >90 for each condition). (G) GFP IHC of sections from the head of Tg(kdrl:GFP) transgenic zebrafish embryos. As expected, inhibition of dll4 increased the EC sprouting activity (G3) but this phenotype was rescued by concomitant knockdown of *eltd1* (G4). Scale bars: 50µm.

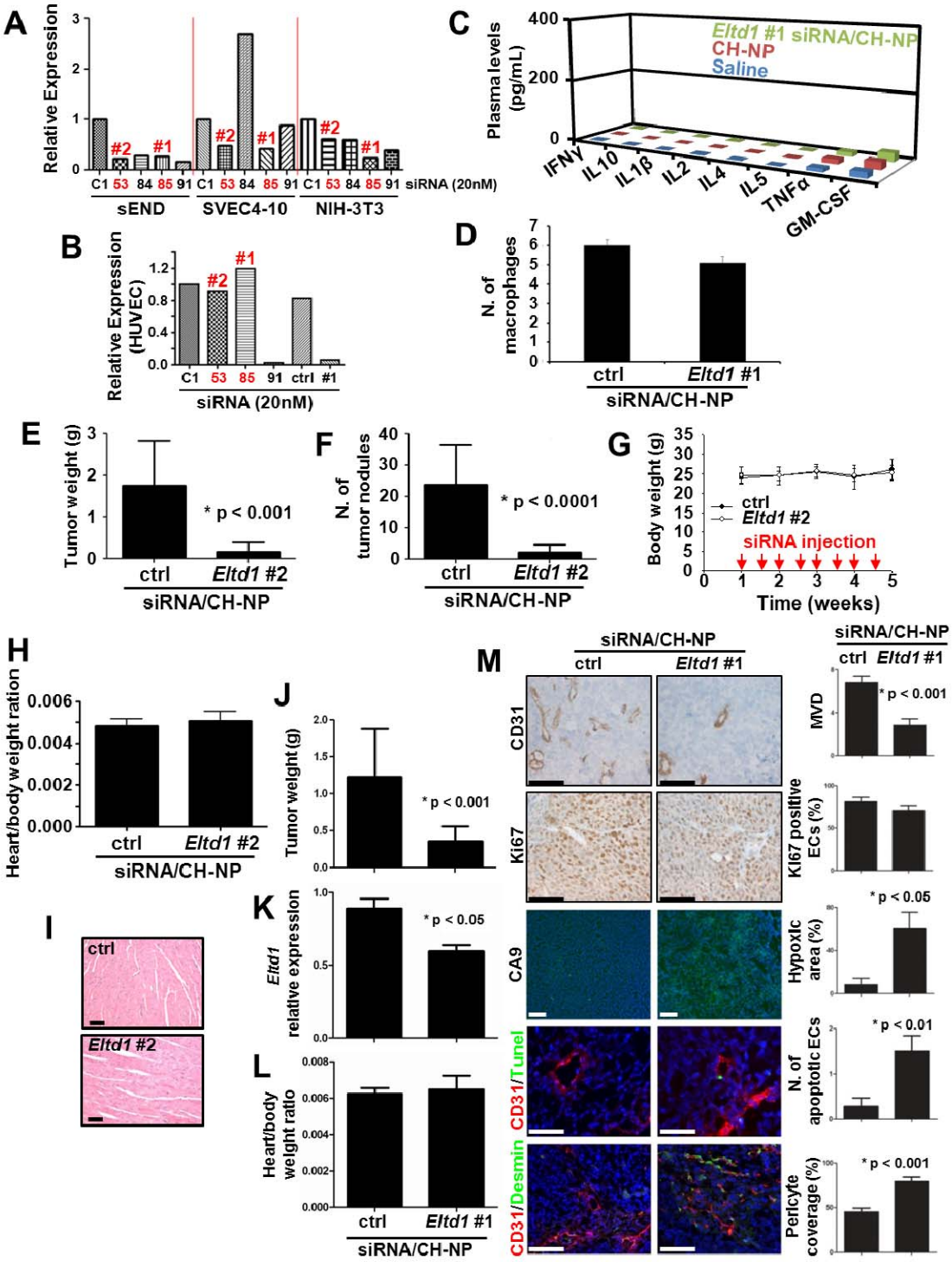

Figure S7, related to Figure 7. ***In vivo Eltd1*** **siRNA treatment in different xenograft models**

(A) Screening of mouse *Eltd1* siRNAs on a panel of murine cell lines. SiRNAs 53, 85 and 91 were then evaluated for possible cross-reactivity with human *ELTD1* by transfecting HUVEC (B). SiRNA ctrl and si *ELTD1* #1 are those previously used for HUVEC experiments. SiRNA #1 (85) and #2 (53) are the murine *Eltd1*-specific siRNA selected for *in vivo* experiments. (C) Evaluation of potential immunostimulatory effects. Mice (n=3 per group) were i.v. injected with a single dose of saline, chitosan nanoparticles (CH-NP), or siRNA/CH-NP and peripheral

blood was collected 12 hours post-injection. Plasma cytokines were measured by ELISA and compared to saline group. (D) Macrophage infiltration in SKOV3ip1 model was not affected by *Eltd1* silencing (cell count performed on CD68 stained xenograft sections). This result is relative to experiment in Figure 7. (E-I) Treatment of SKOV3ip1 tumors with a second *Eltd1* siRNA (#2) shows similar therapeutic effect to those observed with siRNA #1 (Figure 7): reduced tumor weight (E) and decreased number of nodules (F). Analysis on body weight (G), heart/body weight ratio (H) and heart histology (I) did not show any evidence of adverse effects. Similarly, *Eltd1* siRNA (#1)/CH-NP treatment in the HCT116 colorectal s.c. model caused a strong reduction in tumor weight (J), associated to significant *Eltd1* silencing (K) and no effect on heart/body weight ratio (L). At the histological level, we observed reduced MVD (CD31 IHC), associated to increased hypoxia (CA9 IF), EC apoptosis (CD31/Tunel IF) and pericyte coverage (CD31/Desmin IF) (M). All these changes are consistent with observations in the ovarian cancer model. All graph bars represent average ±SEM (unpaired t-test).

Table S5, related to Figure 4. Correlation between ELTD1 endothelial expression and clinical-pathological variables in renal cancer

	Score 1/2	**Score 3/4**	**p value**
Total No. of tumors	39	119	
Gender:			
Female	17	34	0.08
Male	22	85	
Size:	M-W test		0.03 (-ve)
Age:	t-test		0.94
Tumor grade:			
I	6	11	0.54
II	16	57	
III	7	31	
IV	6	15	

Table S6, related to Figure 4. Correlation between ELTD1 endothelial expression and clinical-pathological variables in head and neck cancer

	Score 1/2	**Score 3/4**	**p value**
Total No. of patients	27	37	
Age:	t-test		0.98
Gender:			
Male	4	11	0.16
Female	23	26	
Differentiation:			

Well	2	5	0.23
Moderate	12	22	
Poor	13	10	
pT:			
1	3	4	0.08
2	3	13	
3	3	7	
4	17	13	
pN:			
0	8	16	0.74
1	4	4	
2	13	16	
3	1	1	
UICC Stage:			
I	0	3	0.02
II	0	7	
III	3	3	
IV	23	24	
Smoke:			
Never	3	7	0.59
Ex-smoker	6	9	
Current-smoker	18	20	
Alcohol:			
No	6	7	0.45
Never-heavy	6	14	
Current-heavy	15	16	
Margins:			
> 5mm	7	8	0.14
1mm – 5mm	7	19	

< 1mm	12	10	
Invasive depth:	M – W test		0.48
Invasive front:			
Non-cohesive	12	22	0.32
Cohesive	8	8	
Vascular invasion:			
No	19	25	0.81
Yes	8	12	
Perineural invasion:			
No	14	28	0.03
Yes	13	8	
Postoperative chemotherapy:			
No	24	36	0.30
Yes	3	1	
Post DXT:			
No	8	11	1.00
Yes	19	26	

Table S7, related to Figure 4. Correlation between ELTD1 endothelial expression and clinical-pathological variables in colorectal cancer

	Score 1/2/3	**Score 4**	**p value**
Total number	99	12	
Age:			0.11
Gender:			
Female	45	3	0.18
Male	54	9	
Perforation:			
No	93	12	1.00
Yes	6	0	

Obstruction:			
No	95	11	0.44
Yes	4	1	
pT:			
2	8	3	0.27
3	59	6	
4	32	3	
pN:			
0	57	9	0.30
1	24	3	
2	18	0	
pM:			
0	84	15	0.36
1	15	0	
Lymphatic invasion:			
No	71	10	0.51
Yes	28	2	
Vascular invasion:			
No	62	10	0.16
Yes	37	2	
Stage:			
1, 2	56	9	0.35
3, 4	43	3	
Differentiation:			
0, 1	6	3	0.05
2	77	9	(-ve)
3	16	0	

Supplemental experimental procedures

Gene expression profiling: datasets, data processing and annotation

Head and neck squamous cell carcinoma (HNSCC) and breast cancer (BC) databases of patients treated in Oxford were used together with datasets retrieved from the NCBI Gene Expression Omnibus (http://www.ncbi.nlm.nih.gov/geo/). All details are reported in the following Table. The NCBI database was searched for gene expression datasets in HNSCC, BC and clear cell renal cell carcinoma (CCRCC), whose details had been published in peer-reviewed journals, and where microarray analyses were performed on frozen material extracted before patient treatment.

Eleven datasets (see following Table), encompassing a total of 1250 cases (959 BCs, 121 HNSCCs and 170 CCRCCs), were selected from studies using similar technology platforms (Affymetrix U95, U133 and plus2 arrays) with comparable population demographics per cancer type.

Datasets used for the analysis:

Name	Size	Tumor type	Reference
Vice125	59	HNSCC	(Winter et al., 2007)
GSE2379	20	HNSCC	(Cromer et al., 2004)
GSE6791	42	HNSCC	(Pyeon et al., 2007)
GSE6532Oxf	186	BC	(Loi et al., 2008)
GSE6532KI	149	BC	(Loi et al., 2008)
GSE6532GUY	87	BC	(Loi et al., 2008)
GSE2034	286	BC	(Carroll et al., 2006)
GSE3494	251	BC	(Miller et al., 2005)
GSE15641	32	CCRCC	(Jones et al., 2005)
GSE17816	36	CCRCC	(Dalgliesh et al., 2010)

GSE17818	102	CCRCC	(Dalgliesh et al., 2010)

HNSCC, head and neck squamous cell carcinoma; BC, breast cancer; CCRCC, clear cell renal cell carcinoma

Initial processing of gene expression data was performed for all datasets as described in Buffa et al 2010 (Buffa et al., 2010); specifically, the gcrma function in R was used to estimate expression values, data were quantile-normalized and logged (base2).

Seed clustering

The retrieved microarray datasets were analysed as previously reported in Buffa et al. (BJC; 2010) (Buffa et al., 2010), where a similar approach was used to generate a common hypoxia signature. Specifically, multiple prototype genes (or seeds) were selected on the basis of published evidence of involvement in angiogenesis, and/or expression in vessels, with particular attention to genes upregulated in tumor-associated vessels (see following table). High expression of these genes indicates the presence of a high number of vessels in the specific sample. In this respect, the signature was used as a surrogate marker of MVD to enable identification of a pool of genes possibly involved in the angiogenic process. This is based on the hypothesis that if there is a high MVD there must have been active angiogenesis. These selection criteria were utilized as our aim was to build an angiogenesis profile and study the expression of genes regulated in tumor-associated EC *in vivo*. However, not all genes identified are necessarily directly involved in active angiogenesis and thus further validation is paramount in order to validate the involvement of an individual gene in blood vessel formation. A list of all "seed" genes is presented in the following Table.

Genes selected as initial "seeds" for the seed clustering. Seeds were tested for expression, variability and ability to form a cluster (see methods); only seeds that passed these initial filtering criteria were used to generate the angiogenesis signature (highlighted with red boxes in Figure S1 for each tumor type). A subset of core seeds showed a similar clustering pattern in all tumor types (in red).

Symbol	**Name**	**Function (UniProtKB)**	**Expression in blood vessels/angiogenesis**	**Gene ID**	**Angiogenesis involvement and/or expression in tumor vessels**
TEK (TIE-2)	TEK tyrosine kinase, endothelial	Tyrosine-protein kinase that acts as cell-surface receptor for ANGPT1, ANGPT2 and ANGPT4	EC	7010	(Thomas and Augustin, 2009)

		and regulates angiogenesis, endothelial cell survival, proliferation, migration, adhesion and cell spreading, reorganization of the actin cytoskeleton, but also maintenance of vascular quiescence.			
CDH5	Cadherin 5, type 2 (vascular endothelium)	Cadherins are calcium dependent cell adhesion proteins. This cadherin may play an important role in endothelial cell biology through control of the cohesion and organization of the intercellular junctions. Acts to establish and maintain correct endothelial cell polarity and vascular lumen.	EC	1003	(Cavallaro et al., 2006)
DLL4	Delta-like 4	Plays a role in the Notch signaling pathway by activating Notch-1 and therefore regulating angiogenesis.	EC	54567	(Jubb et al., 2010; Kuhnert et al., 2011; Thurston and Kitajewski, 2008)
EGFL7	EGF-like-domain, multiple 7	Regulates vascular tubulogenesis in vivo. Inhibits platelet-derived growth factor (PDGF)-BB-induced smooth muscle cell migration and promotes endothelial cells adhesion to the substrate in vitro.	EC	51162	(Nichol and Stuhlmann, 2012; Nikolic et al., 2013)
KDR (VEGFR-2)	Kinase insert domain receptor	Tyrosine-protein kinase that acts as a cell-surface receptor for VEGFA, VEGFC and VEGFD. Plays an essential role in the regulation of angiogenesis, vascular development, vascular permeability, and embryonic haematopoiesis. Promotes proliferation, survival, migration and differentiation of endothelial cells.	EC	3791	(Dieterich et al., 2012; Paz and Zhu, 2005; Smith et al., 2010)
ROBO4	Roundabout homolog 4	Receptor for Slit proteins, at least for SLIT2, and seems to be involved in angiogenesis and vascular patterning. May mediate the inhibition of primary endothelial cell migration by Slit proteins.	EC	54538	(Legg et al., 2008)
VWF	Von Willebrand factor	Important in the maintenance of hemostasis, it promotes	EC	7450	(Zanetta et al., 2000)

		adhesion of platelets to the sites of vascular injury by forming a molecular bridge between sub-endothelial collagen matrix and platelets.			
VEZF1	Vascular endothelial zinc finger 1	Transcription factor involved in angiogenesis.	EC	7716	(Miyashita et al., 2004; Zou et al., 2010)
EDIL3	EGF-like repeats and discoidin I-like domains 3 (DEL-1)	Promotes adhesion of endothelial cells through interaction with the alpha-v/beta-3 integrin receptor. Inhibits formation of vascular-like structures. May be involved in regulation of vascular morphogenesis of remodeling in embryonic development.	EC	10085	(Aoka et al., 2002)
PECAM1	Platelet/endothelial cell adhesion molecule (CD31)	Cell adhesion molecule which is required for leukocyte transendothelial migration.	EC	5175	(Cao et al., 2009; Dimaio et al., 2008; Solowiej et al., 2003)
CD34	Hematopoietic progenitor cell antigen CD34	Possible adhesion molecule with a role in early hematopoiesis by mediating the attachment of stem cells to the bone marrow extracellular matrix or directly to stromal cells.	EC	947	Established EC marker
ENG	Endoglin	Major glycoprotein of vascular endothelium. May play a critical role in the binding of endothelial cells to integrins and/or other RGD receptors. Interacts with TGFβ1 and 2 possibly affecting signaling.	EC	2022	(Fonsatti et al., 2010; Marioni et al., 2010; Nassiri et al., 2011; ten Dijke et al., 2008; Uneda et al., 2009)
ESM1	Endothelial cell-specific molecule 1	May have potent implications in lung endothelial cell-leukocyte interactions.	EC	11082	(Chen et al., 2010; Dieterich et al., 2012; Leroy et al., 2010; Roudnicky et al., 2013)
GPR116	G protein-coupled receptor 116	Not known. May have a role in the regulation of acid-base balance	EC	221395	(Wallgard et al., 2008)
SELE	Selectin E	Cell-surface glycoprotein having a role in immunoadhesion. Mediates in the adhesion of blood neutrophils in cytokine-	EC	6401	(Jubeli et al., 2012; Oh et al., 2007; Yu et al., 2004)

		activated endothelium. May have a role in capillary morphogenesis.			
PROM1	Prominin 1 (CD133)	Proposed to play a role in apical plasma membrane organization of epithelial cells. During early retinal development acts as a key regulator of disk morphogenesis. Involved in regulation of MAPK and Akt signaling pathways. In neuroblastoma cells suppresses cell differentiation	-	8842	
VEGFA	Vascular endothelial growth factor A	Growth factor active in angiogenesis, vasculogenesis and endothelial cell growth. Induces endothelial cell proliferation, promotes cell migration, inhibits apoptosis and induces permeabilization of blood vessels.	EC, VSMC/pericyte	7422	(Carmeliet, 2005)
RAMP2	Receptor (G protein-coupled) activity modifying protein 2	Transports the calcitonin gene-related peptide type 1 receptor (CALCRL) to the plasma membrane. Acts as a receptor for adrenomedullin (AM) together with CALCRL.	EC	10266	(Ichikawa-Shindo et al., 2008; Kaafarani et al., 2009)
RGS5	Regulator of G protein signaling 5	Inhibits signal transduction by increasing the GTPase activity of G protein alpha subunits thereby driving them into their inactive GDP-bound form.	EC, VSMC/pericyte	8490	(Furuya et al., 2004; Hamzah et al., 2008)
AGGF1	Angiogenic factor with G patch and FHA domains 1	Promotes angiogenesis and the proliferation of endothelial cells. Able to bind to endothelial cells and promote cell proliferation, suggesting that it may act in an autocrine fashion.	EC, VSMC	55109	(Fan et al., 2009; Lu et al., 2012; Tian et al., 2004)
ITGB3	Integrin, beta 3 (platelet glycoprotein IIIa, antigen CD61)	Integrin alpha-V/beta-3 is a receptor for cytotactin, fibronectin, laminin, matrix metalloproteinase-2, osteopontin, osteomodulin, prothrombin, thrombospondin, vitronectin and von Willebrand factor. Integrin alpha-IIb/beta-3 is a receptor for fibronectin, fibrinogen, plasminogen, prothrombin, thrombospondin and vitronectin. Integrins alpha-IIb/beta-3 and alpha-V/beta-3 recognize the sequence R-G-D in a wide array of ligands.	EC	3690	(Hayashi et al., 2008)

		Integrin alpha-IIb/beta-3 recognizes the sequence H-H-L-G-G-G-A-K-Q-A-G-D-V in fibrinogen gamma chain. Following activation integrin alpha-IIb/beta-3 brings about platelet/platelet interaction through binding of soluble fibrinogen.			
ITGAV	Integrin, alpha V (vitronectin receptor, alpha polypeptide, antigen CD51)	The alpha-V integrins are receptors for vitronectin, cytotactin, fibronectin, fibrinogen, laminin, matrix metalloproteinase-2, osteopontin, osteomodulin, prothrombin, thrombospondin and vWF. They recognize the sequence R-G-D in a wide array of ligands.	EC	3685	(Francois et al., 2012; Nikolic et al., 2013; Santulli et al., 2008)
ITGB5	Integrin, beta 5	Integrin alpha-V/beta-5 is a receptor for fibronectin. It recognizes the sequence R-G-D in its ligand.	EC	3693	(Leifheit-Nestler et al., 2010)
ANGPTL4	Angiopoietin-like 4	Protein with hypoxia-induced expression in endothelial cells. May act as a regulator of angiogenesis and modulate tumorigenesis. Inhibits proliferation, migration, and tubule formation of endothelial cells and reduces vascular leakage. May exert a protective function on endothelial cells through an endocrine action. It is directly involved in regulating glucose homeostasis, lipid metabolism, and insulin sensitivity. In response to hypoxia, the unprocessed form of the protein accumulates in the sub-endothelial extracellular matrix (ECM). The matrix-associated and immobilized unprocessed form limits the formation of actin stress fibers and focal contacts in the adhering endothelial cells and inhibits their adhesion. It also decreases motility of endothelial cells and inhibits the sprouting and tube formation	EC	51129	(Le Jan et al., 2003; Ma et al., 2010; Perdiguero et al., 2011; Tan et al., 2012)

To avoid artefacts arising from low expression and small variability, stringent filtering was applied to the initial seeds. Specifically, to be considered in the analysis seeds needed to be expressed with an average expression higher than the 50^{th} percentile and coefficient of variation greater than 10%, and to be not knowingly affected by cross-hybridization (using Affymetrix annotation data). When multiple probesets matched to the same gene ID, filtering was applied to each of them and correlation between them was estimated. If correlation was significant (Bonferroni adjusted $p<0.05$), then the median expression of all probesets was considered as the expression of the seed gene; if all-but-one probesets were correlated, the median expression of all correlating probesets was used. Otherwise, the probeset with larger absolute expression range was chosen as representative.

Derivation of cancer type-specific and core angiogenesis signatures

These seeds, or prototypes, were used as a starting point from which to build a co-expression network using seed clustering in a meta-analysis context as described previously (Buffa et al., 2010). Briefly, in each dataset a connectivity score, C, is estimated for each gene using bootstrapping techniques; C represents the strength of the relationship between each gene and the whole set of seeds. These scores are thus used in a semi-parametric meta-analysis across datasets to define a gene meta-connectivity score, $\hat{C}$, for each cancer type. Finally, a common signature that is shared between tumor types is derived by considering the meta-connectivity scores product. This is effectively a rank product, as $\hat{C}$ is an average rank. Genes showing a product >0.25 formed the extended common angiogenesis signature (top-ranked in one cancer type and above-average rank in the others), genes with a product >0.9 formed the core signature (top-ranked in all cancers).

The process defines also a shared neighborhood, S, between seeds; S is the number of genes (corrected by the degree of correlation) shared by the seed clusters. Two seeds are considered to carry a high degree of related information if their clusters share many genes (high S); conversely, seeds that show low S ($S<0.5$) with all other seeds are filtered out from the seed clustering.

Compactness of the derived meta-signatures is assessed using an iterative hierarchical clustering method with Bayes information criteria to assess the number of separated clusters (TwoStep clustering, SPSS 15.0). This is an unbiased method to establish numbers of independent clusters

Cell culture, reagents and treatments

Human Umbilical Vein Endothelial Cells (HUVEC) were purchased as a pool (Lonza, Wokingham, UK) or were isolated from fresh human umbilical cords by infusion with 0.2% collagenase (Sigma-Aldrich, Gillingham, UK). HUVEC cells were cultured in M199 (Invitrogen, Paisley, UK) media supplemented with 10% fetal calf serum (FCS; Lonza), 50mg/L ECGS (endothelial cell growth supplement; BD Biosciences, Oxford, UK) and 10U/mL heparin (Sigma-Aldrich). Cells were used between passages 3 and 7. Human umbilical cord Vein Smooth Muscle Cells (HuVSMC; Lonza) were cultured in Medium 231 supplemented with Smooth Muscle growth Supplement (Invitrogen). U87GM (U87, human glioblastoma), sEND (murine EC), SVEC4-10 (murine EC), NIH-3T3 (murine fibroblast), 293T and 293 cells were cultured in DMEM media supplemented with 10% FCS and 1% L-glutamine (Lonza). SKOV3ip1 human epithelial ovarian cancer cells were maintained and propagated in RPMI 1640 supplemented with 15% fetal bovine serum and 0.1% gentamicin sulfate (Gemini Bioproducts, Calabasas, CA). HCT116 colorectal cancer cell line was cultured in McCoy's 5a medium supplemented with 10%FBS. Recombinant human DLL4 (rhDLL4) extracellular domain was purchased from R&D Systems (Minneapolis, USA) and was used to coat tissue culture wells overnight at 4^{o}C at different concentrations in 0.2% gelatin. For cytokine treatments, HUVEC were starved overnight in M199 media with 2% FCS and not supplemented with ECGS. Cells were then stimulated with VEGF (100ng/ml; Invitrogen), bFGF (10ng/ml; Invitrogen), TNFα (10ng/ml; eBIOSCIENCE, Hatfield, UK) or TGFβ2 (10ng/ml; PeproTech, London, UK) for 24h prior to analysis. For cell viability assays, 24h after transfection cells were seeded in 96-well plates (2 x 10^3 and 2.5 x 10^3 cells/well for HUVEC and HuVSMC respectively) in normal culture conditions and tested at 24, 48 and 72h (CellTiter 96 AQ_{ueous} One Solution Cell Proliferation Assay (MTS), Promega, Southampton, UK).

FANTOM4 project CAGE analysis

Results from the FANTOM4 project (http://fantom.gsc.riken.jp/) were used here as further validation of the genes in the meta-signature. A full description of the CAGE methodology and analysis are available via the FANTOM4 project (http://fantom.gsc.riken.jp/4/download/). Briefly, HUVEC grown over rhDLL4 (1μg/ml) or BSA (control) coated plates for 16h were harvested and RNA was extracted and then used for Cap Analysis Gene Expression (CAGE). The CAGE tags were generated and mapped to the genome and clustered to define

transcription start sites (TSS). The TSS have also been mapped to Ensembl transcripts where possible and expression quantified in order to compare the different experimental conditions.

Xenograft tumor models and tissue processing

All protocols were carried out under UK Home Office regulations as previously described (Li et al., 2007). Human glioblastoma U87GM cells (10^7) were subcutaneously implanted into 7 to 8-week-old female BALB/c SCID mice (Harlan Sprague Dawley, Inc., Indiana), 100µl of cell suspension mixed with an equal volume of matrigel (BD Bioscience). Each group consisted of 5 mice. Tumor growth was measured using a caliper and calculated from the formula: "$V = L \times W \times H \times \pi / 0.52$".

Acute drug treatments: when tumors reached the size of 0.35-0.45 cm^3, the mice were treated by intraperitoneal injection (i.p.) of Bevacizumab (10mg/kg body weight), dibenzazepine (DBZ; Syncom Groningen, The Netherlands) (8.1mmol/kg) (Li et al., 2011) or phosphate buffered saline (PBS) as a control. After 3 days, a second dose of Bevacizumab or DBZ was given and, 4h later, the mice were sacrificed and the tumors were collected. Half of each tumor sample was freshly frozen in liquid nitrogen and subsequently used for RNA extraction.

Chronic Bevacizumab treatment: Bevacizumab was injected i.p. every three days at a dose of 10mg/kg, starting when the tumor reached 0.15 cm^3 until the end of the experiment. Animals were sacrificed when the tumors reached the maximal allowed size and samples were collected and freshly frozen in liquid nitrogen.

Microarray analysis of gene expression in xenograft samples

Snap-frozen tissues (5 different tumors per treatment type) were crushed to powder in liquid nitrogen by homogenization. Total RNA was extracted using TRI reagent, as per the manufacturer's instruction. Total RNA was cleaned-up by using Qiagen's RNeasy mini kit. The RNA quality was assessed using RNA 6000 Nano Chips and the Agilent 2100 Bio-analyzer (Agilent Technologies, Paulo Alto, CA). The RNAs with RIN of >7.5 were used for microarray study. cDNA synthesis from each RNA sample, preparation of biotin-labeled cRNA, and hybridization with the GeneChip® Human Genome U133 Plus 2.0 Arrays (to study the human xenograft gene expression; Affymetrix, Santa Clara, CA) or with the Affymetrix mouse 4302 arrays (to study the mouse stromal expression profile; Affymetrix) and laser scanning were performed by the Cancer Research UK Molecular Biology Core Facility Services at the Paterson Institute for Cancer Research, University of Manchester,

Manchester. Data were GCRMA processed, quantile normalized and logged base2. Differential gene expression was assessed between replicate groups using Significance Analysis of Microarrays (samr package in Bioconductor). (Tusher et al., 2001) Any probesets that exhibited an adjusted p value <0.05 were called differentially expressed. For the purpose of this study only data regarding genes in our meta-signature are presented.

Patients demographic and histopathological features

A. Renal cancer

Total		N=158
Age (year)	Medial (range)	64 (36 – 87)
Gender	Male	51 (31%)
	Female	107 (68%)
pT	1	52
	2	28
	3	76
pN	0	33
	1	8
	2	1
Tumor grade (Fuhrman)	1	17
	2	73
	3	38
	4	22
Histotype	Clear Cell Carcinoma	125
	Papillary Carcinoma	27
	Others	4

B. Colorectal cancer

Total		N=111
Age (year)	Medial (range)	72.3 (25 – 96)
Gender	Male	63 (57%)
	Female	48 (43%)

Perforation	No	105 (95%)
	Yes	6
Obstruction	No	106
	Yes	5
pT	1	1
	2	10
	3	65
	4	35
pN	0	66
	1	27
	2	18
pM	No	96
	Yes	15
Lymphatic invasion	No	81
	Yes	30
Vascular invasion	No	72
	Yes	39
Differentiation	0	3
	1	6
	2	86
	3	16
Mucinous	No	102
	Yes	5
Stage	1	10
	2	55
	3	35
	4	11

C. Head and Neck cancer

Total		N=64
Age (year)	Medial (range)	64 (43 – 92)
Gender	Male	50 (77%)
	Female	15 (23%)
pT	1	7
	2	16
	3	10
	4	31
pN	0	24
	1	8
	2	30
	3	2
UICC stage	1	3
	2	7
	3	6
	4	48
Differentiation	Well	7
	Mod	35
	Poor	23

Immunohistochemistry and immunofluorescence analysis

IHC of primary human tissues: ELTD1 staining was performed using an anti-human ELTD1 antibody (Ab; HPA025229 from Sigma-Aldrich) recognizing the extracellular domain of the protein. In brief, paraffin-embedded slides were de-waxed and antigen retrieved by microwaving in 50mM Tris-2mM EDTA (pH 9.0). Sections were incubated with the Ab (1:500; about 1μg/ml) at room temperature for 45 minutes. Bound Ab was detected using the Envision system (DAKOCytomation, Ely, Cambridgeshire, UK), visualized by using 2,3-diaminobenzidine chromogen and counterstained with hematoxilin. Matched samples were stained in parallel

and tonsil sections were used as controls. Cores were scored for ELTD1 immunolabeling intensity on a semi quantitative scale. The vascular staining correlated with clinico-pathological data was specifically endothelial cell expression, identified histologically as the most adluminal cell in a vessel (vascular smooth muscle cell staining was not scored). Vessels surrounded by tumor were selected for scoring. Negative staining was reported as score 0, scores 1-4 were used for increasing intensity of ELTD1. The highest score among replicates (2 cores for colorectal samples) was considered as representative. In survival analysis, the cut-off score was chosen based on the discrete value more likely to differentiate between normal and tumoral levels.

CD31 staining was performed using an anti-human CD31 antibody (JC70A from DAKO; 1µg/ml; citrate buffer pH 6.0). MVD was then scored by counting the number of CD31 positive vessels per TMA core (only whole cores were scored).

IF of primary human tissues: FFPE tissue sections were de-waxed, antigen-retrieved and permeabilized as already described and co-stained with anti-ELTD1 (1:500) and either anti-CD34 (1:100; QBEnd/10; Novus Biologicals LLC, Littleton, CO, USA) or Cy3- conjugated anti α-smooth muscle actin (α-SMA; 1A4; Sigma-Aldrich). Secondary fluorescent antibodies were purchased from Invitrogen. Pictures were taken using a wide field digital fluorescence microscope (Zeiss, Germany).

IHC and IF of xenografts: IHC analysis for cell proliferation (Ki67, 1:200, Zymed), microvessel density (MVD, CD31, 1:500, Pharmingen), macrophage number (CD68, 1:400, Serotec) and hypoxia (carbonic anhydrase Anti-CA9, 1:500, Novus), and IF for apoptosis (TUNEL, 1:200, Promega) and pericyte coverage (CD31/desmin, 1:500 and 1:200, Abcam) were all performed as described previously (Lu et al., 2010; Thaker et al., 2006). For statistical analyses, sections from five randomly selected tumors per group were stained and 5 random fields per tumor were scored. Pictures were taken at x200 or x100 magnification. All stainings were quantified by 2 investigators in a blinded fashion.

***In vitro* RNA interference and cDNA transfection**

ELTD1-specific small interfering RNAs (siRNAs) and negative control with similar GC content (medium GC content) were transfected at a final concentration of 20nM using RNAiMAX reagent (all by Invitrogen). siRNA sequences are: siELTD1#1 5'-GGGCUGUGAGCUGACAUACUCAAAU-3' and siELTD1#2 5'-CAAUCAUUGCCGGACUGCUACACUA-3'. Cells were transfected at 30-50% confluency in Opti-MEM I Reduced

Serum Medium with GlutaMAX I (Invitrogen). Mouse *Eltd1*-specific siRNAs and relative negative controls (all from Sigma-Aldrich) were transfected into murine cell lines or HUVEC with the same protocol used for human *ELTD1*-specific siRNAs. An *ELTD1*-coding expression plasmid (IMAGE Clone 5229055 corresponding to GenBank accession number BC025721; Source BioScience LifeSciences, UK) was used to transfect 293 cells using Lipofectamine 2000 reagent (Invitrogen) according to manufacturer's instructions. A plasmid coding for N-terminally Flag-tagged ELTD1 was generated (cloning details available upon request) and used to transfect 293T cells for surface expression analysis.

Flow cytometry analysis

24h after transfection with a Flag-ELTD1/IRES/EGFP plasmid, 293T cells were washed with PBS and harvested with PBS-EDTA 5mM. Cells were then immunolabeled with a mouse anti-Flag primary antibody (Sigma-Aldrich) and subsequently stained with an anti-mouse APC-conjugated secondary antibody (Invitrogen). Samples were acquired on a FACSCalibur with CellQuest software and data were analysed with FlowJo software.

RNA extraction, reverse transcription and quantitative PCR

Total RNA from cell cultures was isolated using the RNeasy mini kit (Qiagen, Crawley, West Sussex, UK) according to the manufacturer's instructions. Complementary DNA (cDNA) was synthesized from 0.5-1µg of total RNA using Superscript III first-strand system (Invitrogen). Quantitative PCR (qPCR) analysis was performed in triplicate using the SYBR GreenER qPCR SuperMix Universal (Invitrogen) and Chromo4 fluorescence detector (MJ Research, Waltham, MA, USA). Relative quantification was done using the ΔΔCt method normalizing to β2-microglobulin gene expression. For primer sequences see following Table.

qPCR primers		
Gene		sequence 5' - 3'
β2-microglobulin	forward	TGCTGTCTCCATGTTTGATGTATCT
	reverse	TCTCTGCTCCCCACCTCTAAGT
CD93	forward	GCGAAGAGGGAGGAGAAGAA
	reverse	GTCCCAGGTGTCGGACTGTA
DCHS1	forward	CTACAATGCCTCACTGCCTGA
	reverse	CAAGTCCAGCACCCAAGGAAT
EDNRB	forward	GCGAATCTGCTTGCTTCATCC
	reverse	CCAATGGCAAGCAGAAATAGAAAC
ELTD1	forward	GCTCAAACCCACCCACATTAT
	reverse	CACAGCCCTCTGAAGACCAG
FZD4	forward	CTCATCCAGTACGGCTGCTC
	reverse	GCCAATGGGGATGTTGATCTTC

GPR116	forward	TCCCCAAGGAGAACCACTTT
	reverse	CCTCAGTGCCTCTTCACCAG
GPR124	forward	GCTGCTGAACTTGTGCTTCC
	reverse	CAGCGTGGATAGGGAGGAGT
HEY2	forward	GGCGTCGGGATCGGATAAAT
	reverse	GCGTGTGCGTCAAAGTAGCG
LMO2	forward	GCGCCTCTACTACAAACTGG
	reverse	TCCGCTTGTCACAGGATGC
RGS5	forward	CGTGATTCCCTGGACAAACTC
	reverse	CCTCACAGGCAATCCAGAAC
CD97	forward	AGCTATACCTGCCAGTGCCT
	reverse	ATTCACATCTGTGCAGACCTTCG
EMR1	forward	CAGGGAGGTACAAGTGCAGC
	reverse	GGCACTCATTGATATCAGTACAGGA
EMR2	forward	AACACCCTCGGCAGCTACA
	reverse	TTCATTCACATCTGTGCAGAGCTTC
EMR3	forward	GGAAAGGTGGTTGGCTTACGG
	reverse	GAAAGCAGAGGCCTGGAAGAAG
EMR4	forward	GCACTGCAGTTGCCCTATCA
	reverse	GTGCCGCTCACAACGTAAGA
eltd1	forward	CCAAGGAGAAAGGCTGCACAT
	reverse	TGAGGATAGCAAGGGACCAATG
actin	forward	ATGCTCTCCCTCACGCCATC
	reverse	CACGCACGATTTCCCTCTCA

Western Blotting

Cells were lysed in RIPA buffer and 5-10µg of proteins were separated by sodium dodecyl sulfate–polyacrylamide gel electrophoresis (SDS-PAGE) on 4-12% gradient gels (Invitrogen) and then transferred by conventional semidry blotting. Anti-ELTD1 (1:1000) and anti β-actin (1:20,000) were both from Sigma-Aldrich. Horseradish peroxidase (HRP)-conjugated secondary Abs were purchased from DAKO and labeling was detected using the enhanced chemiluminescence (ECL) reagent (GE Healthcare, Chalfont St Giles, UK). Non-denaturing conditions were also used according to the blue native gel technique following manufacturer's instructions (Invitrogen).

3D *in vitro* sprouting angiogenesis assay

HUVEC spheroids of defined cell number (500-1000 cells) were generated by the hanging-drop method (Korff and Augustin, 1998). Briefly, 4h after siRNA transfection, cells were harvested and re-suspended in culture medium containing 0.20% (wt/vol) carboxymethylcellulose and seeded in non-adherent round-bottom 60-well mini trays (Nunc). 16-24h later, spheroids were collected and embedded into 200µl of matrigel (BD

Biosciences). After polymerization, spheroids were cultured for 24h in the presence of EBM2 medium and growth supplements (EGM2 bullet kit, cat. number CC-3162, Lonza). Thereafter, angiogenesis was quantified by counting the number of sprouts for each spheroid and the 20 spheroids with the most sprouts per condition were considered for statistical analysis. Although the standard protocol contains collagen as the extracellular matrix, and VEGF or bFGF as single factors to induce sprouting, matrigel was selected for the reasons described in the adhesion assay (Supplemental Information). In a set of experiments, 4h after transfection cells were pre-labeled with viable fluorescent dyes according to manufacturer's protocol (cell tracker green, cat. number C2925, and blue, cat. number C2111; Invitrogen). Spheroids were generated by mixing control and ELTD1 knockdown cells in a 1:1 ratio and both color combinations were analysed. Spheroids were then embedded into 150µl of matrigel and plated on glass-bottom dishes (MatTek, Ashland, MA, USA). After 24h, spheroids were fixed over night at 4^{o}C in 4% formaldehyde-PBS and pictures of the sprouts were taken using a confocal microscope (Zeiss LSM 510 META). The number of tip and stalk cells of each color were counted.

Adhesion assay

24h after siRNA transfection, 10 x 10^{3} cells were seeded on 55µl of matrigel in 96-well plate wells. Cells were left to adhere for 30 minutes before being extensively washed with PBS to remove all not adhering ones. After fixing with 4% formaldehyde-PBS a low magnification picture was taken at the center of each well. Cells number was then quantified by image analysis using Image J software (Image J website, rsbweb.nih.gov). Cell adhesion to matrigel, a complex extracellular matrix produced by tumor cells was studied because the ELTD1 ligand is unknown and we wanted to recapitulate a tumor-like context.

Wound healing assay

After siRNA transfection, cells were allowed to grow until confluent, before a cross ("wound") was made by scraping the cell monolayer with a P200 pipette tip in the center of the well. Pictures of the wound were taken at the four arms of the cross at different time points until complete coverage was achieved. The open wound surface was then quantified by image analysis using Image J software

Zebrafish husbandry, *eltd1* probe generation and whole mount *in situ* hybridization

Wild-type (WT) and transgenic Tg(kdrl:GFP) (Beis et al., 2005; Huang et al., 2003) embryos and adult fish were raised and maintained as described (Westerfield, 1993).

The 700bp *eltd1* cDNA was amplifyed from a 27hpf cDNA using the PCR primers 5'-GTTATACATCGCCAGCAGGGCCC-3' and 5'-TCACCCGCTGCTGCATAGCG-3', followed by subcloning into the pGEM-T easy vector (Promega). Antisense mRNA was transcribed from the cDNA template linearized with *Sac*II using SP6 RNA polymerase. Whole mount *in situ* hybridization on zebrafish embryos was carried out as previously described (Jowett and Yan, 1996). Antisense RNA probes were transcribed from linearized templates in the presence of digoxigenin (Roche). DIG antibody was detected using BM-Purple (Roche).

Morpholino (MO) injection in zebrafish embryos

MO targeting the pre-mRNA of *eltd1* were designed by Genetools: *eltd1* ATGMO 5'-CATTGGAGAACTGTGTAAAAACTCC-3' (2.75ng/embryo) and *eltd1* spliceMO 5'-ATATATGCCAAACCTCTACAATCGC-3', which targets the exon 2/intron 2 splice-donor site (12ng/embryo). To validate the efficiency of the *eltd1* spliceMO, RT-PCR was performed on cDNA collected at 27hpf from WT and *eltd1* spliceMO injected embryos, using the following primers: 5'-ACTCCTGCTTTTCGCTGCTTGGT-3' (which binds exon1/2) and 5'-GGTCACATCGTTCAGTGGAAGCGT-3' (which binds exon 9), amplifying a correctly spliced product of 1162bp. *Dll4* MO (5'-TGATCTCTGATTGCTTACGTTCTTC-3') was injected at 12ng/embryo (Hogan et al., 2009).

Embryo imaging

Images were obtained on a Nikon SMZ 1500 zoom stereomicroscope using a Nikon DXM 1200 digital camera (Nikon, UK). GFP^+ embryos were visualised using a Leica MZ FLIII fluorescence stereomicroscope (Leica Microsystems, UK) and photographed with a Hamamatsu ORCA-ER camera driven by Simple PCI 5.1.0.0110 (Compix, USA). Confocal images were obtained using a Zeiss LSM 510 META confocal laser microscope, and 3D projections were generated using Zeiss LSM (Carl Zeiss Inc). Images were processed with Adobe Photoshop CS4 (Adobe Systems, San Jose, CA).

SUPPLEMENTAL REFERENCES (not cited in the main manuscript)

Aoka, Y., Johnson, F. L., Penta, K., Hirata Ki, K., Hidai, C., Schatzman, R., Varner, J. A., and Quertermous, T. (2002). The embryonic angiogenic factor Del1 accelerates tumor growth by enhancing vascular formation. Microvascular research *64*, 148-161.

Beis, D., Bartman, T., Jin, S. W., Scott, I. C., D'Amico, L. A., Ober, E. A., Verkade, H., Frantsve, J., Field, H. A., Wehman, A.*, et al.* (2005). Genetic and cellular analyses of zebrafish atrioventricular cushion and valve development. Development *132*, 4193-4204.

Cao, G., Fehrenbach, M. L., Williams, J. T., Finklestein, J. M., Zhu, J. X., and Delisser, H. M. (2009). Angiogenesis in platelet endothelial cell adhesion molecule-1-null mice. The American journal of pathology *175*, 903-915.

Carmeliet, P. (2005). VEGF as a key mediator of angiogenesis in cancer. Oncology *69 Suppl 3*, 4-10.

Carroll, J. S., Meyer, C. A., Song, J., Li, W., Geistlinger, T. R., Eeckhoute, J., Brodsky, A. S., Keeton, E. K., Fertuck, K. C., Hall, G. F.*, et al.* (2006). Genome-wide analysis of estrogen receptor binding sites. Nat Genet *38*, 1289-1297.

Cavallaro, U., Liebner, S., and Dejana, E. (2006). Endothelial cadherins and tumor angiogenesis. Experimental cell research *312*, 659-667.

Chen, L. Y., Liu, X., Wang, S. L., and Qin, C. Y. (2010). Over-expression of the Endocan gene in endothelial cells from hepatocellular carcinoma is associated with angiogenesis and tumour invasion. The Journal of international medical research *38*, 498-510.

Cromer, A., Carles, A., Millon, R., Ganguli, G., Chalmel, F., Lemaire, F., Young, J., Dembele, D., Thibault, C., Muller, D.*, et al.* (2004). Identification of genes associated with tumorigenesis and metastatic potential of hypopharyngeal cancer by microarray analysis. Oncogene *23*, 2484-2498.

Dalgliesh, G. L., Furge, K., Greenman, C., Chen, L., Bignell, G., Butler, A., Davies, H., Edkins, S., Hardy, C., Latimer, C.*, et al.* (2010). Systematic sequencing of renal carcinoma reveals inactivation of histone modifying genes. Nature *463*, 360-363.

Dimaio, T. A., Wang, S., Huang, Q., Scheef, E. A., Sorenson, C. M., and Sheibani, N. (2008). Attenuation of retinal vascular development and neovascularization in PECAM-1-deficient mice. Developmental biology *315*, 72-88.

Fan, C., Ouyang, P., Timur, A. A., He, P., You, S. A., Hu, Y., Ke, T., Driscoll, D. J., Chen, Q., and Wang, Q. K. (2009). Novel roles of GATA1 in regulation of angiogenic factor AGGF1 and endothelial cell function. The Journal of biological chemistry *284*, 23331-23343.

Fonsatti, E., Nicolay, H. J., Altomonte, M., Covre, A., and Maio, M. (2010). Targeting cancer vasculature via endoglin/CD105: a novel antibody-based diagnostic and therapeutic strategy in solid tumours. Cardiovascular research *86*, 12-19.

Francois, P., Bertos, N., Laferriere, J., Sadekova, S., Souleimanova, M., Zhao, H., Finak, G., Meterissian, S., Hallett, M. T., and Park, M. (2012). Gene-expression profiling of microdissected breast cancer microvasculature identifies distinct tumor vascular subtypes. Breast cancer research : BCR *14*, R120.

Furuya, M., Nishiyama, M., Kimura, S., Suyama, T., Naya, Y., Ito, H., Nikaido, T., and Ishikura, H. (2004). Expression of regulator of G protein signalling protein 5 (RGS5) in the tumour vasculature of human renal cell carcinoma. The Journal of pathology *203*, 551-558.

Hamzah, J., Jugold, M., Kiessling, F., Rigby, P., Manzur, M., Marti, H. H., Rabie, T., Kaden, S., Grone, H. J., Hammerling, G. J.*, et al.* (2008). Vascular normalization in Rgs5-deficient tumours promotes immune destruction. Nature *453*, 410-414.

Hayashi, H., Sano, H., Seo, S., and Kume, T. (2008). The Foxc2 transcription factor regulates angiogenesis via induction of integrin beta3 expression. The Journal of biological chemistry *283*, 23791-23800.

Huang, C. J., Tu, C. T., Hsiao, C. D., Hsieh, F. J., and Tsai, H. J. (2003). Germ-line transmission of a myocardium-specific GFP transgene reveals critical regulatory elements in the cardiac myosin light chain 2 promoter of zebrafish. Dev Dyn *228*, 30-40.

Ichikawa-Shindo, Y., Sakurai, T., Kamiyoshi, A., Kawate, H., Iinuma, N., Yoshizawa, T., Koyama, T., Fukuchi, J., Iimuro, S., Moriyama, N.*, et al.* (2008). The GPCR modulator protein RAMP2 is essential for angiogenesis and vascular integrity. The Journal of clinical investigation *118*, 29-39.
Jones, J., Otu, H., Spentzos, D., Kolia, S., Inan, M., Beecken, W. D., Fellbaum, C., Gu, X., Joseph, M., Pantuck, A. J.*, et al.* (2005). Gene signatures of progression and metastasis in renal cell cancer. Clinical cancer research : an official journal of the American Association for Cancer Research *11*, 5730-5739.
Jowett, T., and Yan, Y. L. (1996). Double fluorescent in situ hybridization to zebrafish embryos. TIG *12*, 387-389.
Jubb, A. M., Soilleux, E. J., Turley, H., Steers, G., Parker, A., Low, I., Blades, J., Li, J. L., Allen, P., Leek, R.*, et al.* (2010). Expression of vascular notch ligand delta-like 4 and inflammatory markers in breast cancer. The American journal of pathology *176*, 2019-2028.
Jubeli, E., Moine, L., Vergnaud-Gauduchon, J., and Barratt, G. (2012). E-selectin as a target for drug delivery and molecular imaging. Journal of controlled release : official journal of the Controlled Release Society *158*, 194-206.
Kaafarani, I., Fernandez-Sauze, S., Berenguer, C., Chinot, O., Delfino, C., Dussert, C., Metellus, P., Boudouresque, F., Mabrouk, K., Grisoli, F.*, et al.* (2009). Targeting adrenomedullin receptors with systemic delivery of neutralizing antibodies inhibits tumor angiogenesis and suppresses growth of human tumor xenografts in mice. FASEB journal : official publication of the Federation of American Societies for Experimental Biology *23*, 3424-3435.
Korff, T., and Augustin, H. G. (1998). Integration of endothelial cells in multicellular spheroids prevents apoptosis and induces differentiation. J Cell Biol *143*, 1341-1352.
Kuhnert, F., Kirshner, J. R., and Thurston, G. (2011). Dll4-Notch signaling as a therapeutic target in tumor angiogenesis. Vascular cell *3*, 20.
Le Jan, S., Amy, C., Cazes, A., Monnot, C., Lamande, N., Favier, J., Philippe, J., Sibony, M., Gasc, J. M., Corvol, P., and Germain, S. (2003). Angiopoietin-like 4 is a proangiogenic factor produced during ischemia and in conventional renal cell carcinoma. The American journal of pathology *162*, 1521-1528.
Legg, J. A., Herbert, J. M., Clissold, P., and Bicknell, R. (2008). Slits and Roundabouts in cancer, tumour angiogenesis and endothelial cell migration. Angiogenesis *11*, 13-21.
Leifheit-Nestler, M., Conrad, G., Heida, N. M., Limbourg, A., Limbourg, F. P., Seidler, T., Schroeter, M. R., Hasenfuss, G., Konstantinides, S., and Schafer, K. (2010). Overexpression of integrin beta 5 enhances the paracrine properties of circulating angiogenic cells via Src kinase-mediated activation of STAT3. Arteriosclerosis, thrombosis, and vascular biology *30*, 1398-1406.
Leroy, X., Aubert, S., Zini, L., Franquet, H., Kervoaze, G., Villers, A., Delehedde, M., Copin, M. C., and Lassalle, P. (2010). Vascular endocan (ESM-1) is markedly overexpressed in clear cell renal cell carcinoma. Histopathology *56*, 180-187.
Li, J. L., Sainson, R. C., Shi, W., Leek, R., Harrington, L. S., Preusser, M., Biswas, S., Turley, H., Heikamp, E., Hainfellner, J. A., and Harris, A. L. (2007). Delta-like 4 Notch ligand regulates tumor angiogenesis, improves tumor vascular function, and promotes tumor growth in vivo. Cancer research *67*, 11244-11253.
Loi, S., Haibe-Kains, B., Desmedt, C., Wirapati, P., Lallemand, F., Tutt, A. M., Gillet, C., Ellis, P., Ryder, K., Reid, J. F.*, et al.* (2008). Predicting prognosis using molecular profiling in estrogen receptor-positive breast cancer treated with tamoxifen. BMC Genomics *9*, 239.
Lu, Q., Yao, Y., Liu, S., Huang, Y., Lu, S., Bai, Y., Zhou, B., Xu, Y., Li, L., Wang, N.*, et al.* (2012). Angiogenic factor AGGF1 promotes therapeutic angiogenesis in a mouse limb ischemia model. PloS one *7*, e46998.
Ma, T., Jham, B. C., Hu, J., Friedman, E. R., Basile, J. R., Molinolo, A., Sodhi, A., and Montaner, S. (2010). Viral G protein-coupled receptor up-regulates Angiopoietin-like 4 promoting angiogenesis and vascular permeability in Kaposi's sarcoma. Proceedings of the National Academy of Sciences of the United States of America *107*, 14363-14368.

Marioni, G., D'Alessandro, E., Giacomelli, L., and Staffieri, A. (2010). CD105 is a marker of tumour vasculature and a potential target for the treatment of head and neck squamous cell carcinoma. Journal of oral pathology & medicine : official publication of the International Association of Oral Pathologists and the American Academy of Oral Pathology *39*, 361-367.
Miller, L. D., Smeds, J., George, J., Vega, V. B., Vergara, L., Ploner, A., Pawitan, Y., Hall, P., Klaar, S., Liu, E. T., and Bergh, J. (2005). An expression signature for p53 status in human breast cancer predicts mutation status, transcriptional effects, and patient survival. Proceedings of the National Academy of Sciences of the United States of America *102*, 13550-13555.
Miyashita, H., Kanemura, M., Yamazaki, T., Abe, M., and Sato, Y. (2004). Vascular endothelial zinc finger 1 is involved in the regulation of angiogenesis: possible contribution of stathmin/OP18 as a downstream target gene. Arteriosclerosis, thrombosis, and vascular biology *24*, 878-884.
Nassiri, F., Cusimano, M. D., Scheithauer, B. W., Rotondo, F., Fazio, A., Yousef, G. M., Syro, L. V., Kovacs, K., and Lloyd, R. V. (2011). Endoglin (CD105): a review of its role in angiogenesis and tumor diagnosis, progression and therapy. Anticancer research *31*, 2283-2290.
Nichol, D., and Stuhlmann, H. (2012). EGFL7: a unique angiogenic signaling factor in vascular development and disease. Blood *119*, 1345-1352.
Nikolic, I., Dudvarski Stankovic, N., Bicker, F., Meister, J., Braun, H., Awwad, K., Baumgart, J., Simon, K., Thal, S. C., Patra, C*., et al.* (2013). EGFL7 ligates alphavbeta3 integrin to enhance vessel formation. Blood.
Oh, I. Y., Yoon, C. H., Hur, J., Kim, J. H., Kim, T. Y., Lee, C. S., Park, K. W., Chae, I. H., Oh, B. H., Park, Y. B., and Kim, H. S. (2007). Involvement of E-selectin in recruitment of endothelial progenitor cells and angiogenesis in ischemic muscle. Blood *110*, 3891-3899.
Paz, K., and Zhu, Z. (2005). Development of angiogenesis inhibitors to vascular endothelial growth factor receptor 2. Current status and future perspective. Frontiers in bioscience : a journal and virtual library *10*, 1415-1439.
Perdiguero, E. G., Galaup, A., Durand, M., Teillon, J., Philippe, J., Valenzuela, D. M., Murphy, A. J., Yancopoulos, G. D., Thurston, G., and Germain, S. (2011). Alteration of developmental and pathological retinal angiogenesis in angptl4-deficient mice. The Journal of biological chemistry *286*, 36841-36851.
Pyeon, D., Newton, M. A., Lambert, P. F., den Boon, J. A., Sengupta, S., Marsit, C. J., Woodworth, C. D., Connor, J. P., Haugen, T. H., Smith, E. M*., et al.* (2007). Fundamental differences in cell cycle deregulation in human papillomavirus-positive and human papillomavirus-negative head/neck and cervical cancers. Cancer research *67*, 4605-4619.
Roudnicky, F., Poyet, C., Wild, P., Krampitz, S., Negrini, F., Huggenberger, R., Rogler, A., Stohr, R., Hartmann, A., Provenzano, M*., et al.* (2013). Endocan Is Upregulated on Tumor Vessels in Invasive Bladder Cancer Where It Mediates VEGF-A-Induced Angiogenesis. Cancer research *73*, 1097-1106.
Santulli, R. J., Kinney, W. A., Ghosh, S., Decorte, B. L., Liu, L., Tuman, R. W., Zhou, Z., Huebert, N., Bursell, S. E., Clermont, A. C*., et al.* (2008). Studies with an orally bioavailable alpha V integrin antagonist in animal models of ocular vasculopathy: retinal neovascularization in mice and retinal vascular permeability in diabetic rats. The Journal of pharmacology and experimental therapeutics *324*, 894-901.
Smith, N. R., Baker, D., James, N. H., Ratcliffe, K., Jenkins, M., Ashton, S. E., Sproat, G., Swann, R., Gray, N., Ryan, A*., et al.* (2010). Vascular endothelial growth factor receptors VEGFR-2 and VEGFR-3 are localized primarily to the vasculature in human primary solid cancers. Clinical cancer research : an official journal of the American Association for Cancer Research *16*, 3548-3561.
Solowiej, A., Biswas, P., Graesser, D., and Madri, J. A. (2003). Lack of platelet endothelial cell adhesion molecule-1 attenuates foreign body inflammation because of decreased angiogenesis. The American journal of pathology *162*, 953-962.
Tan, M. J., Teo, Z., Sng, M. K., Zhu, P., and Tan, N. S. (2012). Emerging roles of angiopoietin-like 4 in human cancer. Molecular cancer research : MCR *10*, 677-688.

ten Dijke, P., Goumans, M. J., and Pardali, E. (2008). Endoglin in angiogenesis and vascular diseases. Angiogenesis *11*, 79-89.
Thaker, P. H., Han, L. Y., Kamat, A. A., Arevalo, J. M., Takahashi, R., Lu, C., Jennings, N. B., Armaiz-Pena, G., Bankson, J. A., Ravoori, M.*, et al.* (2006). Chronic stress promotes tumor growth and angiogenesis in a mouse model of ovarian carcinoma. Nat Med *12*, 939-944.
Thomas, M., and Augustin, H. G. (2009). The role of the Angiopoietins in vascular morphogenesis. Angiogenesis *12*, 125-137.
Thurston, G., and Kitajewski, J. (2008). VEGF and Delta-Notch: interacting signalling pathways in tumour angiogenesis. British journal of cancer *99*, 1204-1209.
Tian, X. L., Kadaba, R., You, S. A., Liu, M., Timur, A. A., Yang, L., Chen, Q., Szafranski, P., Rao, S., Wu, L.*, et al.* (2004). Identification of an angiogenic factor that when mutated causes susceptibility to Klippel-Trenaunay syndrome. Nature *427*, 640-645.
Tusher, V. G., Tibshirani, R., and Chu, G. (2001). Significance analysis of microarrays applied to the ionizing radiation response. Proc Natl Acad Sci U S A *98*, 5116-5121.
Uneda, S., Toi, H., Tsujie, T., Tsujie, M., Harada, N., Tsai, H., and Seon, B. K. (2009). Anti-endoglin monoclonal antibodies are effective for suppressing metastasis and the primary tumors by targeting tumor vasculature. International journal of cancer Journal international du cancer *125*, 1446-1453.
Westerfield, M. (1993). The Zebrafish Book: A Guide for the Laboratory use of Zebrafish (Brachydanio rerio), (Eugene, OR: University of Oregon Press).
Winter, S. C., Buffa, F. M., Silva, P., Miller, C., Valentine, H. R., Turley, H., Shah, K. A., Cox, G. J., Corbridge, R. J., Homer, J. J.*, et al.* (2007). Relation of a hypoxia metagene derived from head and neck cancer to prognosis of multiple cancers. Cancer research *67*, 3441-3449.
Yu, Y., Moulton, K. S., Khan, M. K., Vineberg, S., Boye, E., Davis, V. M., O'Donnell, P. E., Bischoff, J., and Milstone, D. S. (2004). E-selectin is required for the antiangiogenic activity of endostatin. Proceedings of the National Academy of Sciences of the United States of America *101*, 8005-8010.
Zanetta, L., Marcus, S. G., Vasile, J., Dobryansky, M., Cohen, H., Eng, K., Shamamian, P., and Mignatti, P. (2000). Expression of Von Willebrand factor, an endothelial cell marker, is up-regulated by angiogenesis factors: a potential method for objective assessment of tumor angiogenesis. International journal of cancer Journal international du cancer *85*, 281-288.
Zou, Z., Ocaya, P. A., Sun, H., Kuhnert, F., and Stuhlmann, H. (2010). Targeted Vezf1-null mutation impairs vascular structure formation during embryonic stem cell differentiation. Arteriosclerosis, thrombosis, and vascular biology *30*, 1378-1388.